DNA: A Programmable Force Sensor

Christian Albrecht *et al.*

Science **301**, 367 (2003);
DOI: 10.1126/science.1084713

Science (print ISSN 0036-8075; online ISSN 1095-9203) is published weekly, except the last week in December, by the American Association for the Advancement of Science, 1200 New York Avenue NW, Washington, DC 20005.

9. D. M. Wellik, P. J. Hawkes, M. R. Capecchi, *Genes Dev.* **16**, 1423 (2002).
10. G. M. Wahba, S. L. Hostikka, E. M. Carpenter, *Dev. Biol.* **231**, 87 (2001).
11. D. M. Wellik, M. R. Capecchi, data not shown.
12. S. L. Hostikka, M. R. Capecchi, *Mech. Dev.* **70**, 133 (1998).
13. Y. Herault, J. Beckers, M. Gerard, D. Duboule, *Dev. Biol.* **208**, 157 (1999).
14. P. Dolle, J. C. Izpisua-Belmonte, H. Falkenstein, A. Renucci, D. Duboule, *Nature* **342**, 767 (1989).
15. P. Dolle, J. C. Izpisua-Belmonte, J. M. Brown, C. Tickle, D. Duboule, *Genes Dev.* **5**, 1767 (1991).
16. B. Favier *et al.*, *Development* **122**, 449 (1996).
17. M. Suzuki, A. Kuroiwa, *Mech. Dev.* **118**, 241 (2002).
18. M. Hildebrand, *Analysis of Vertebrate Structure* (Wiley, New York, ed. 4, 1995).
19. E. B. Lewis, *Nature* **276**, 565 (1978).
20. M. J. Cohn, C. Tickle, *Nature* **399**, 474 (1999).
21. M. Kmita, B. Tarchini, D. Duboule, Y. Harault, *Development* **129**, 5521 (2002).
22. We are indebted to S. L. Hostikka for preparation of the *Hoxc10* and *Hoxc11* mutant mice, and we thank J. F. Fallon, S. Sakonju, and B. W. Bisgrove for discussions of these data before publication.

Supporting Online Material
www.sciencemag.org/cgi/content/full/301/5631/363/DC1
SOM Text
References

14 April 2003; accepted 9 June 2003

DNA: A Programmable Force Sensor

Christian Albrecht,[1] Kerstin Blank,[1] Mio Lalic-Mülthaler,[1] Siegfried Hirler,[1] Thao Mai,[1] Ilka Gilbert,[1] Susanne Schiffmann,[1] Tom Bayer,[1] Hauke Clausen-Schaumann,[1]* Hermann E. Gaub[2]

Direct quantification of biomolecular interaction by single-molecule force spectroscopy has evolved into a powerful tool for materials and life sciences. We introduce an approach in which the unbinding forces required to break intermolecular bonds are measured in a differential format by comparison with a known reference bond (here, a short DNA duplex). In addition to a marked increase in sensitivity and force resolution, which enabled us to resolve single–base pair mismatches, this concept allows for highly specific parallel assays. This option was exploited to overcome cross-reactions of antibodies in a protein biochip application.

Within the past decade, a variety of experimental tools based on applying and measuring piconewton forces between single molecules have been developed and have contributed to a better understanding of the mechanics of biomolecules and molecular bonds (*1*–*4*). Force measurements reveal detailed insights into binding-potential landscapes and into functional aspects of the molecules under investigation, and as a result, force has become a new structural and functional parameter in materials and life sciences. Receptor-ligand pairs (*5*–*8*), protein and nucleic acid structures (*9*–*15*), and even covalent bonds (*16*) have been investigated, and it has become evident that biomolecular processes are governed by piconewton forces. However, two major bottlenecks have hindered the widespread use of single-molecule mechanics: sizable instrumental effort and limited force resolution. To our knowledge, no single–base pair mismatch detection by single-molecule force measurements has been reported, despite numerous efforts. The best resolution to date has been 10 base pairs (bp), obtained by shearing and unzipping short oligomers by atomic force micoscopy (AFM) (*17*, *18*).

In conventional single-molecule force spectroscopy, inter- or intramolecular forces are exerted and measured with microscopic force sensors like AFM cantilevers or beads in optical or magnetic traps (*19*, *20*). With state-of-the-art instrumentation, the force resolution is limited only by thermal fluctuations that are detected by the force sensor. Arguments based on the fluctuation-dissipation theorem predict that a reduction of the sensor size should improve the signal-to-noise ratio (*21*). This has been verified in experimental studies using a new generation of small AFM cantilevers (*22*). The logical extrapolation is to replace the cantilever by a single elastic molecule. To increase the precision of the assay even further, we chose a differential measurement format, where rupture forces of two molecular complexes are directly compared with each other. This differential format offers several advantages. Because of the high symmetry of the assay, most external disturbances cancel out (*23*). In addition, for most applications, a precise measure of the difference is more valuable than two absolute values with their respective error bars, such as the ranking of binders or a single–base pair mismatch detection in a DNA sequence.

In our setup (Fig. 1), the cantilever spring was replaced by a polymeric anchor and a known molecular bond (reference bond) carrying a fluorescence label. The molecular bond under investigation was directly compared to this reference bond, which served as a molecular force standard. During separation of the two surfaces, the polymeric anchor was stretched, and the force acting along the molecular chain consisting of the sample and labeled reference complex built up gradually, until the weaker of the two bonds ruptured. The difference in the stability of the two bonds breaks the symmetry in this experiment. As a result, there is a higher probability that the fluorescence label will end up on the side of the stronger bond rather than on the side of the weaker bond. This process can be seen as a 1-bit analog-to-digital conversion broadened by thermal fluctuations (*24*). Many single-molecule force measurements can be performed simultaneously, using two congruent chip surfaces and different spots containing the molecules of interest. Counting the labels on each side, for instance, by single-molecule optics, provides a quantitative measure for the differences between the distributions of the bond rupture probabilities of the two molecular complexes. It is equivalent to measuring the fluorescence intensities, which are proportional to the densities of the fluorescence labels (*25*). Although a large number of molecules are probed simultaneously, the actual force measurement is still performed at the single-molecule level, because each sample bond is probed individually by a single reference bond.

Figure 1B illustrates the setup schematically. The rupture forces of two DNA strands with different hybridization lengths (a 20-bp duplex and a 25-bp duplex) are directly compared. Both oligonucleotides are bridged with a conjugated 65-base oligonucleotide, carrying a terminal Cy5 fluorescent label. The resulting 20-bp duplex is coupled to an activated glass surface, and the 25-bp duplex to a soft polydimethylsiloxane (PDMS) stamp (*26*–*28*), both by means of polyethylene glycol (PEG) spacers. Figure 1C shows fluorescence images of the glass surface containing the capture oligonucleotide and the labeled sample oligonucleotide before the two surfaces were brought into contact and separated again, and both glass (bottom) and PDMS (top) after the separation of the two surfaces. Because the PDMS stamp has a grid pattern of trenches to ease the water flux at the surface during separation, the transferred labels form a checkerboard pattern on the PDMS. No transfer occurred in the trenches, so that here the initial label density was maintained on the glass surface, whereas in the contact areas (squares), labels were transferred from the glass to the PDMS side.

[1]Nanotype GmbH, Lochhamer Schlag 12, 82166 Gräfelfing, Germany. [2]Lehrstuhl für Angewandte Physik and Center for Nano-Science, Amalienstrasse 54, 80799 München, Germany.

*To whom correspondence should be addressed. E-mail: hauke.clausen-schaumann@nanotype.de

A direct quantification of the fluorescent label density is limited by the different optical and chemical properties of the two surfaces—glass chip and PDMS stamp—which influence the quantum yield and the excitation efficiency of the label. In addition, the coupling efficiencies to the two chip surfaces may differ. However, the symmetry of the experiment can be restored by placing the two molecules of interest on the same side of the assay and measuring both against a common reference on the other side (*29*). This is the format chosen for the following experiments, where single–base pair mismatches and different binding modes of DNA were investigated. A quantitative analysis of the experiment that is shown in Fig. 1 is provided in fig. S1.

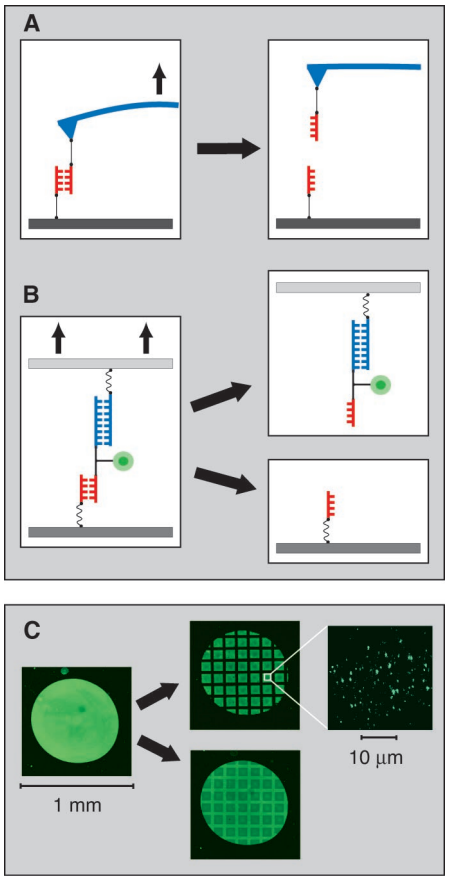

Fig. 1. (**A**) Conventional, AFM-based single-molecule force spectroscopy, in which the rupture force required to break a molecular bond, such as a DNA duplex (red), is measured with a cantilever spring (blue). (**B**) The differential force test, in which the rupture force of a sample bond (red) is measured by comparing it with a known reference bond (blue), which serves as a molecular force standard. Upon loading the chain of polymer spacers, sample bond, and reference bond, the weaker bond has a higher probability of rupturing than the stronger one. Consequently, most of the probed fluorescence labels (green) end up with the stronger bond after separating the two surfaces. (**C**) (left) Cy5 fluorescence image of a spot containing the molecular chains of polymer spacers, sample, and reference duplexes before connecting the biotinylated reference duplexes to the second chip surface. (middle) Cy5 fluorescence image of both chip surfaces—microstructured PDMS (top) and glass (bottom)—after separating them again. (right) PDMS surface at single-molecule resolution after separating the two surfaces. The image was obtained by TIRF.

To investigate the force resolution of the differential force test, we measured the reduction of the unbinding forces caused by a single–base pair mismatch in a 20-bp DNA duplex. Figure 2A illustrates the experimental setup and shows the superposition of the histograms of fluorescence intensities, obtained on the PDMS surface, after separating the two chips. The main peaks of the two histograms are clearly separated and are to a good approximation of Gaussian shape, indicating a homogeneous surface coverage with statistical distribution of the bond-rupture process. The spike (to the left) stems from the trenches of the grid and reflects the fluorescence background. The mean fluorescence intensities were determined by fitting Gaussian distributions to the histogram peaks. The ratio of these intensities, which directly represents the ratio of the bond-rupture probabilities of mismatch to perfect match was found to be 1.7. Because the half width of the two peaks is less than one-third of the difference of the peak values, a quantitative single-nucleotide polymorphism assay with high precision is possible. The experiment was conducted in a buffer solution containing 150 mM NaCl at room temperature. Under these conditions, thermal off-rates are extremely low (*30*), and discrimination between mismatch and perfect match sequences is difficult to obtain in conventional equilibrium binding assays (*31*, *32*). This high thermal stability ensures that in the force-based assay, the data are not obscured by spontaneous strand-separation events or differences in hybridization efficiencies (*33*).

On conventional DNA chips, single–base pair mismatches are detected by identifying differences in the thermal off-rate or the equilibrium constant. In both cases, stringent conditions are established by reducing the salt concentration (or alternatively increasing temperature) such that the DNA duplexes to be analyzed either dissociate at different time scales or bind with distinguishable binding ratios (*34*). Because both ionic strength and temperature are global parameters, a delicate compromise of these parameters has to be chosen to establish satisfactory ambient conditions for all the different spots on the chip. These global boundary conditions impose severe limitations on the sequences that can be tested in parallel on the same chip and require large numbers of additional control spots (*35*, *36*). In contrast, in the differential force for-

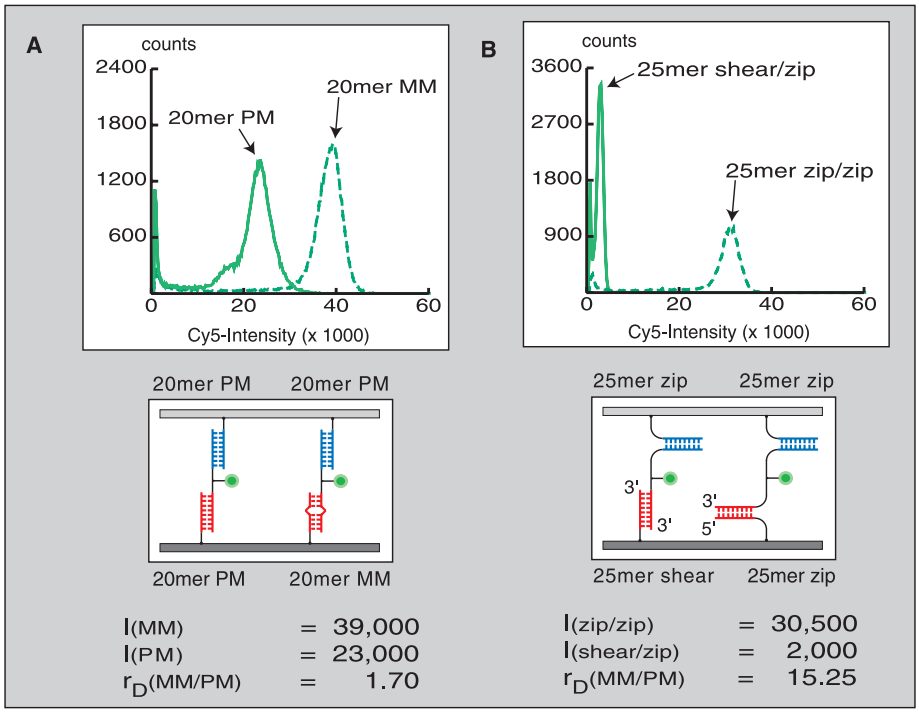

Fig. 2. (**A**) Histograms of a perfectly matching (PM) 20-bp DNA duplex (left) as compared with a 20-bp duplex that has a single–base pair mismatch (MM). Both duplexes were probed with a 20-bp reference complex that is reverse to the perfectly matching 20-bp duplex. Both sample duplexes are identical, except for a single base mutation (G → C) that was introduced at position 13 of the capture oligonucleotide. (**B**) Histograms of identical 25-bp DNA duplexes in both shear (left) and unzip geometry (right), both of which have been probed with an identical 25-bp duplex in unzip geometry. I, mean fluorescence intensity; r_D, discrimination ratio.

mat, the stringency imposed by the reference complex is a local boundary condition. Both the sequence and the length of the reference complex on the stamp may be chosen for every sample spot on the chip accordingly, allowing optimum force resolution and background discrimination for every spot. Thermodynamic stringency is global, whereas mechanical stringency is local. The combination of maximum resolution and local stringency is desirable for the precise quantification of interactions.

Figure 2B highlights an additional and unique feature of force-based assays: the discrimination among energetically and kinetically equivalent interactions. Both hybrids, the one in shear geometry and the one in unzip geometry, have identical sequences and, therefore, have the same binding energy, as well as the same thermal on-rates and off-rates. However, upon forced dissociation, the complex in unzip geometry has a probability of rupturing that is more than 15 times as high as that of the complex in shear geometry, as can be derived from the peak positions of the histograms in Fig. 2B. This pronounced difference is consistent with earlier measurements (*13*, *17*, *37*, *38*) in which unzipping forces of 14 pN and values that were more than three times as high for the shear geometry were measured under comparable conditions (*39*).

The discrimination between different binding modes, as illustrated above, and the concept of mechanical stringency offer striking advantages when applied to the field of protein arrays. In this field, it is crucial to discriminate between specific and nonspecific interactions, and it is difficult to define a common set of stringent ambient conditions for many different proteins (*40*, *41*). Proteins typically interact with each other specifically over well-defined binding sites, whereas nonspecific interactions with other proteins and with surfaces occur over larger surface areas (*42*). As shown in Fig. 2B, discrimination between these two binding modes can then be reliably achieved using a low-force but high-affinity force sensor, such as a DNA duplex in unzip conformation. Figure 3 shows that the threshold force defined by such a DNA duplex in unzipping geometry is well suited to discriminate between specific and nonspecific binding for a variety of antibody-antigen interactions. At the same time, the affinity is high enough to provide a stable anchor. The antibodies can be safely "delivered" to their respective antigens. In addition, if needed, other threshold forces can easily be programmed into the DNA reference complex by changing the base composition or the binding geometry.

The advantages of the force-based delivery of antibodies become more apparent when applied to capture arrays based on a sandwich format. In conventional sandwich arrays, each detection antibody can interact with all spots of the array. Therefore, each analyte molecule that is bound to the array can be decorated by detection antibodies, even the ones that are bound nonspecifically or because of cross-reactive capture antibodies (*43*). Consequently, the nonspecific background and the number of false-positives grow geometrically with the number of spots on the chip, which severely limits the multiplexing capabilities of protein capture arrays (*44*). The differential force assay allows for the local application of specific detection antibodies, and the second chip surface therefore provides for a second dimension of specific encoding (*45*). Figure 4 shows an example of a cross-reactive capture antibody that is specific for both human and murine interleukin-5 (IL-5). In a conventional protein array, discrimination between human and murine antigens is not possible (Fig. 4A) with this capture antibody, and the assay generates false-positive results (*46*). In our assay, the second chip surface (top surface) allows the definition of two specific spots for the two different antigens, even if the same cross-reactive capture antibody is used in both spots of the capture surface (bottom). Specific detection and reliable discrimination of both antigens are now possible in a single step. This illustrates the potential of our assay to overcome a major bottleneck in the field of protein biochips, namely, the lack of specificity caused by nonspecific interactions and cross-reactions (*47*, *48*).

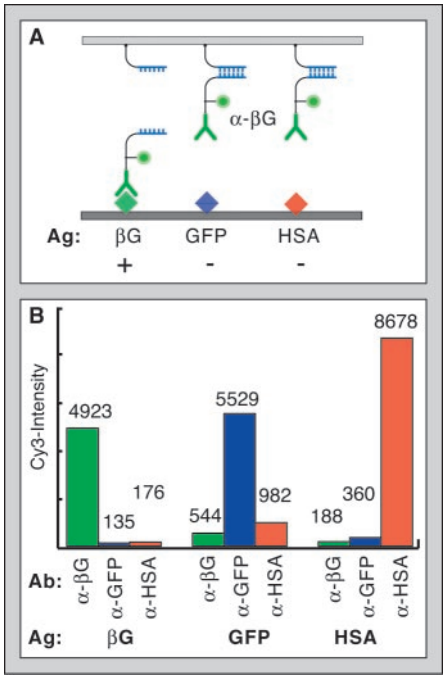

Fig. 3. Discrimination between specific and nonspecific antibody-antigen interactions with a DNA force sensor. (**A**) Three spots with different proteins [β-galactosidase (βG), green fluorescent protein (GFP), and human serum albumin (HSA)] on the bottom surface were probed with antibodies to β-galactosidase, which were connected to the top surface by way of DNA force sensors in unzipping conformation. Upon separation of the two surfaces, only β-galactosidase, which was probed with its specific antibody, was decorated with the fluorescently labeled antibody. (**B**) Fluorescence intensities (arbitrary units) on three different antigens (on the bottom surface) after each antigen was probed with three different antibodies, which were connected to the top surface by way of DNA zippers. Ab, antibody; Ag, antigen.

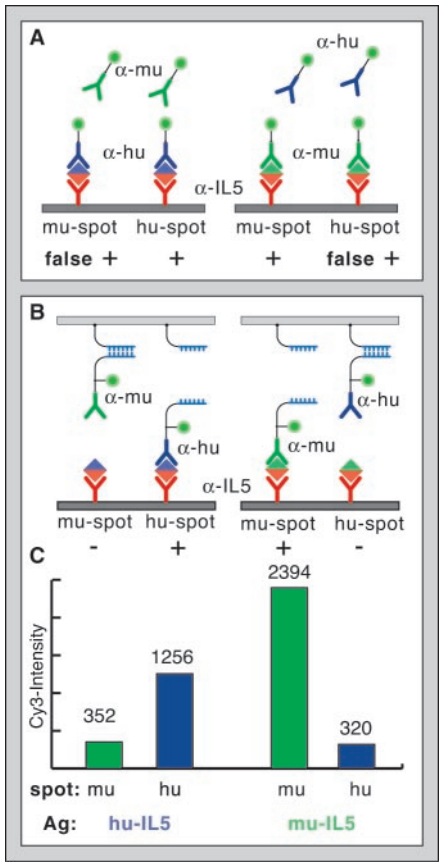

Fig. 4. Antibodies to IL-5, which bind both murine IL-5 and human IL-5, were used as capture antibodies in a sandwich immunoassay. The detection antibodies are specific for either murine IL-5 or human IL-5. (**A**) If both detection antibodies are applied simultaneously in buffer solution, as in a conventional protein array, the discrimination between murine (mu) and human (hu) antigens is not possible, because of the cross-reactivity of the capture antibody. (**B**) If the detection antibodies are coupled to the top surface by way of DNA force sensors, they can be applied locally. The second chip surface provides a second dimension for specific encoding, making it possible to define a murine and a human spot on the array and to discriminate between the two antigens. (**C**) Fluorescence intensities on the murine spots (green) and the human spots (blue) after incubation of human (left) and murine (right) antigen. Ag, antigen.

References and Notes

1. C. Bustamante, J. C. Macosko, G. J. Wuite, *Nature Rev. Mol. Cell Biol.* **1**, 130 (2000).
2. H. Clausen-Schaumann, M. Seitz, R. Krautbauer, H. E. Gaub, *Curr. Opin. Chem. Biol.* **4**, 524 (2000).

3. R. Merkel, *Phys. Rep.* **346**, 343 (2001).
4. R. Lavery, A. Lebrun, J.-F. Allemand, D. Bensimon, V. Croquette, *J. Phys. Cond. Matter* **14**, R383 (2002).
5. V. T. Moy, E.-L. Florin, H. E. Gaub, *Science* **266**, 257 (1994).
6. E.-L. Florin, V. T. Moy, H. E. Gaub, *Science* **264**, 415 (1994).
7. R. Merkel, P. Nassoy, A. Leung, K. Ritchie, E. Evans, *Nature* **397**, 50 (1999).
8. F. Schwesinger *et al.*, *Proc. Natl. Acad. Sci. U.S.A.* **97**, 9972 (2000).
9. S. B. Smith, Y. Cui, C. Bustamante, *Science* **271**, 795 (1996).
10. M. S. Kellermayer, S. B. Smith, H. L. Granzier, C. Bustamante, *Science* **276**, 1112 (1997).
11. M. Rief, M. Gautel, F. Oesterhelt, J. M. Fernandez, H. E. Gaub, *Science* **276**, 1109 (1997).
12. A. F. Oberhauser, P. E. Marszalek, H. P. Erickson, J. M. Fernandez, *Nature* **393**, 181 (1998).
13. M. Rief, H. Clausen-Schaumann, H. E. Gaub, *Nature Struct. Biol.* **6**, 346 (1999).
14. F. Oesterhelt *et al.*, *Science* **288**, 143 (2000).
15. T. Hugel *et al.*, *Science* **296**, 1103 (2002).
16. M. Grandbois, M. Beyer, M. Rief, H. Clausen-Schaumann, H. E. Gaub, *Science* **283**, 1727 (1999).
17. T. Strunz, K. Oroszlan, R. Schafer, H. J. Guntherodt, *Proc. Natl. Acad. Sci. U.S.A.* **96**, 11277 (1999).
18. R. Krautbauer, M. Rief, H. E. Gaub, *Nano Lett.* **3**, 493 (2003).
19. A. Janshoff, M. Neitzert, Y. Oberdorfer, H. Fuchs, *Angew. Chem. Int. Ed.* **39**, 3212 (2000).
20. A. D. Mehta, M. Rief, J. A. Spudich, D. A. Smith, R. M. Simmons, *Science* **283**, 1689 (1999).
21. F. Gittes, C. F. Schmidt, *Eur. Biophys. J.* **27**, 75 (1998).
22. M. B. Viani *et al.*, *J. Appl. Phys.* **86**, 2258 (1999).
23. In conventional force spectroscopy, molecular forces are measured as displacements against spring constants or trap slopes. Because the nature of intra- and intermolecular forces is fundamentally different from metal or silicon springs (or from optical or magnetic traps), all kinds of fluctuations or drifts, such as temperature and pH, will alter the measured signal. In the differential molecular format, each cancels out the effects of the other.
24. As long as the sample and reference complexes are similar, for example, consisting of two antibodies or two DNA oligomers (as in our case), the potential-energy landscape of the two complexes will be comparable. This means that the difference of the unbinding forces is approximately independent of the rate at which the force was built up. Consequently, this assay format is insensitive to variations of the spacer length or to separation velocity. Also, the force threshold of the common reference has to lie either within the force window defined by the molecular bonds under investigation, or close to one of these forces. The force distributions are broadened by thermal fluctuations on the order of k_BT/l , where k_B is Boltzmann's constant, T is temperature, and l is the characteristic width of the binding potential. Consequently, the window of possible reference forces is broadened by approximately the same amount (*49*, *50*).
25. This is true as long as the lateral density is kept below the fluorescence resonance energy transfer limit.
26. A. Kumar, N. L. Abbott, E. Kim, H. A. Biebuyck, G. M. Whitesides, *Acc. Chem. Res.* **28**, 219 (1995).
27. Y. Xia, G. M. Whitesides, *Annu. Rev. Mater. Sci.* **28**, 153 (1998).
28. A. Bernard, B. Michel, E. Delamarche, *Anal. Chem.* **73**, 8 (2001).
29. Different optical and chemical properties, as well as differences in coupling efficiencies to the two surfaces, are compensated in this way.
30. D. Pörschke, M. Eigen, *J. Mol. Biol.* **62**, 361 (1971).
31. C. Schildkraut, S. Lifson, *Biopolymers* **3**, 195 (1965).
32. P. Nollau, C. Wagener, *J. Int. Fed. Clin. Chem.* **9**, 162 (1997).
33. The discrimination between mismatch and perfect match could clearly be improved by decreasing the salt concentration or increasing the temperature and making use of both spontaneous and force-induced strand separation. However, in this study, we focused on forced unbinding events.
34. M. Chee *et al.*, *Science* **274**, 610 (1996).
35. R. J. Lipshutz, S. P. Fodor, T. R. Gingeras, D. J. Lockhart, *Nature Genet.* **21**, 20 (1999).
36. F. Naef, D. A. Lim, N. Patil, M. Magnasco, *Phys. Rev. E.* **65**, 040902 (2002).
37. U. Bockelmann, B. Essevaz-Roulet, F. Heslot, *Phys. Rev. Lett.* **79**, 4489 (1997).
38. B. Essevaz-Roulet, U. Bockelmann, F. Heslot, *Proc. Natl. Acad. Sci. U.S.A.* **94**, 11935 (1997).
39. The difference in the bond-rupture probabilities of the two chosen unbinding geometries is much larger than the difference in unbinding forces. Our assay measures the ratio of unbinding probabilities directly. Therefore, differences down to the order of the thermal force scale k_BT/l can be resolved.
40. R. P. Ekins, *J. Pharm. Biomed. Anal.* **7**, 155 (1989).
41. R. P. Ekins, F. Chu, *Trends Biotechnol.* **12**, 89 (1994).
42. P. Mitchell, *Nature Biotechnol.* **20**, 225 (2002).
43. L. G. Mendoza *et al.*, *Biotechniques* **27**, 778 (1999).
44. A. Abbott, *Nature* **415**, 112 (2002).
45. H. Petach, L. Glod, *Curr. Opin. Biotechnol.* **13**, 309 (2002).
46. C. Abrecht *et al.*, data not shown.
47. G. MacBeath, *Nature Genet.* **32** (suppl. 2), 526 (2002).
48. P. Cutler, *Proteomics* **3**, 3 (2003).
49. E. Evans, K. Ritchie, *Biophys. J.* **72**, 1541 (1997).
50. P. Hänggi, P. Talkner, M. Borkovec, *Rev. Mod. Phys.* **62**, 251 (1990).

51. We thank M. Rief for kindly providing the total internal reflection flourescence (TIRF) data showing single-molecule fluorescence, M. Benoit for technical support, F. Oesterhelt, C. Duschl, and D. Mendik for helpful discussions. Supported by the Nanobiotechnology and Proteomics program of the Bundesministerium für Bildung and Forschung (grants 13N8141 and O312821A) and the Bayerische Forschungsstiftung.

Supporting Online Material

www.sciencemag.org/cgi/content/full/301/5631/367/DC1

Materials and Methods

Fig. S1

19 March 2003; accepted 13 June 2003

Allosteric Activators of Glucokinase: Potential Role in Diabetes Therapy

Joseph Grimsby,[1] Ramakanth Sarabu,[1] Wendy L. Corbett,[1] Nancy-Ellen Haynes,[1] Fred T. Bizzarro,[1] John W. Coffey,[1] Kevin R. Guertin,[1] Darryl W. Hilliard,[1]* Robert F. Kester,[1] Paige E. Mahaney,[1]† Linda Marcus,[1] Lida Qi,[1] Cheryl L. Spence,[1] John Tengi,[1] Mark A. Magnuson,[2] Chang An Chu,[1] Mark T. Dvorozniak,[1] Franz M. Matschinsky,[3] Joseph F. Grippo[1]‡

Glucokinase (GK) plays a key role in whole-body glucose homeostasis by catalyzing the phosphorylation of glucose in cells that express this enzyme, such as pancreatic β cells and hepatocytes. We describe a class of antidiabetic agents that act as nonessential, mixed-type GK activators (GKAs) that increase the glucose affinity and maximum velocity (V_{max}) of GK. GKAs augment both hepatic glucose metabolism and glucose-induced insulin secretion from isolated rodent pancreatic islets, consistent with the expression and function of GK in both cell types. In several rodent models of type 2 diabetes mellitus, GKAs lowered blood glucose levels, improved the results of glucose tolerance tests, and increased hepatic glucose uptake. These findings may lead to the development of new drug therapies for diabetes.

Glucose homeostasis is lost in type 2 diabetes because of combined defects in both insulin secretion and insulin action (*1*, *2*). The characterization of patients with abnormal glycemic control due to either gain- or loss-of-function mutations in GK has provided new insights into the pathogenesis of type 2 diabetes. Loss-of-function mutations in the gene encoding GK have been linked to maturity-onset diabetes of the young type 2 (MODY2), an autosomal dominant form of diabetes mellitus characterized by early onset and mild chronic fasting hyperglycemia (*3*, *4*). MODY2 patients display impaired glucose responsiveness of β cells, decreased net accumulation of glycogen, and increased hepatic glucose production after meals (*5*, *6*). The GK mutations found in MODY2 patients result in decreased activity of this enzyme as a result of reduction in its V_{max} and/or reduced affinity toward its substrates, glucose and adenosine triphosphate (ATP) (*7*–*11*). In contrast, gain-of-function GK mutations, which increase the catalytic activity of GK, cause persistent hyperinsulinemic hypoglycemia of infancy as a result of lowering the threshold

[1]Department of Metabolic Diseases, Hoffmann-La Roche Inc., Nutley, NJ 07110, USA. [2]Department of Molecular Physiology and Biophysics, Vanderbilt University, Nashville, TN 37232, USA. [3]Department of Biochemistry and Diabetes Center, University of Pennsylvania School of Medicine, Philadelphia, PA 19104, USA.

*Present address: Lilly Research Laboratories, Lilly Corporate Center, Indianapolis, IN 46285, USA.

†Present address: Chemical Sciences, Wyeth Research, 500 Arcola Road, Collegeville, PA 19426, USA.

‡To whom correspondence should be addressed. E-mail: joseph.grippo@roche.com